Supporting Information

Derivation of flux equation based on model in Fig. S1.

The normalized population of each state under steady state conditions was calculated by first setting the total rate of change of each state to zero as in Eq. A1;

$$\text{Eq. A1. } \frac{d[A]}{dt} = \frac{d[BH_2]}{dt} = \frac{d[BH_3]}{dt} = \frac{d[CH_2]}{dt} = \frac{d[CH_3]}{dt} = 0$$

which yields the following system of linear equations Eq. A2 – Eq. A6:

Eq. A2 – Eq. A6:

$$0 = \frac{d[A]}{dt} = -k_1[H_O]^2[A] + k_{-1}[BH_2]$$

$$0 = \frac{d[BH_2]}{dt} = k_1[H_O]^2[A] - (k_{-1} + k_3[H_O] + k_5[H_I] + k_2)[BH_2] + (k_{-3} + k_{-5})[BH_3] + k_{-2}[CH_2]$$

$$0 = \frac{d[BH_3]}{dt} = (k_3[H_O] + k_5[H_I])[BH_2] - (k_{-3} + k_{-5} + k_4)[BH_3] + k_{-4}[CH_3]$$

$$0 = \frac{d[CH_2]}{dt} = k_2[BH_2] - (k_{-2} + k_7[H_O] + k_9[H_I])[CH_2] + (k_{-7} + k_{-9})[CH_3]$$

$$0 = \frac{d[CH_3]}{dt} = k_4[BH_3] - (k_{-4} + k_{-7} + k_{-9})[CH_3] + (k_7[H_O] + k_9[H_I])[CH_2]$$

Solving the system using Maxima (*1*) or Mathematica (*2*) yielded the populations of each state of the protein under steady-state kinetic conditions as a function of the rate constants and $[H_I]$ and $[H_O]$; the populations were normalized to reflect an unchanging amount of total protein.

Inward proton flux at a given pH_{in} and pH_{out} was defined by subtracting the difference of extraviral proton release and binding rates from the difference of intraviral proton release and binding rates, as follows in Eq. A7:

Eq. A7. $Flux = (Release,in - Binding,in) - (Release,out - Binding,out)$

Or, more specifically defined for this system in Eq. A8:

Eq. A8. $Flux = (k_{-9}[CH_3]+k_{-5}[BH_3])-(k_9[H_1][CH_2]+k_5[H_1][BH_2])-$

$((k_{-7}[CH_3]+k_{-3}[BH_3]+k_{-1}[BH_2])-(k_1[A][H_O]^2+k_3[BH_2][H_O]+k_7[CH_2][H_O]))$

where the protein terms are the normalized steady-state populations obtained from solving the linear system described above. In the more complex model discussed below, flux was described similarly by summing all possible internal deprotonation event rates as the "Release, in" term, all possible internal protonation event rates as the "Binding, in" term, etc.

Conceptual framework for electrical distances.

Relative electrical distances in the flux models were based on the approach of Lear (*3*), but expanded to include additional minima and barriers corresponding to both conformational changes and protonation transitions. Net barriers only were fit for the BH_2-CH_2 conformational change. Rate constants included to represent "leak" processes were initially modeled as voltage-independent, as were conformational transitions involving fully deprotonated tetramer.

Calculation of population-averaged pK_a over two conformational states.

The population-averaged pK_a was calculated according to Eq. A9, where $K_{a,x}$ and $K_{a,y}$ represent the acid dissociation constant values of conformational states *x* and *y*, and K_{eq} represents the equilibrium constant for conversion of *yH* to *xH*.

Eq. A9 $$K_{a,avg} = \frac{K_{a,y} + K_{eq}K_{a,x}}{1 + K_{eq}}$$

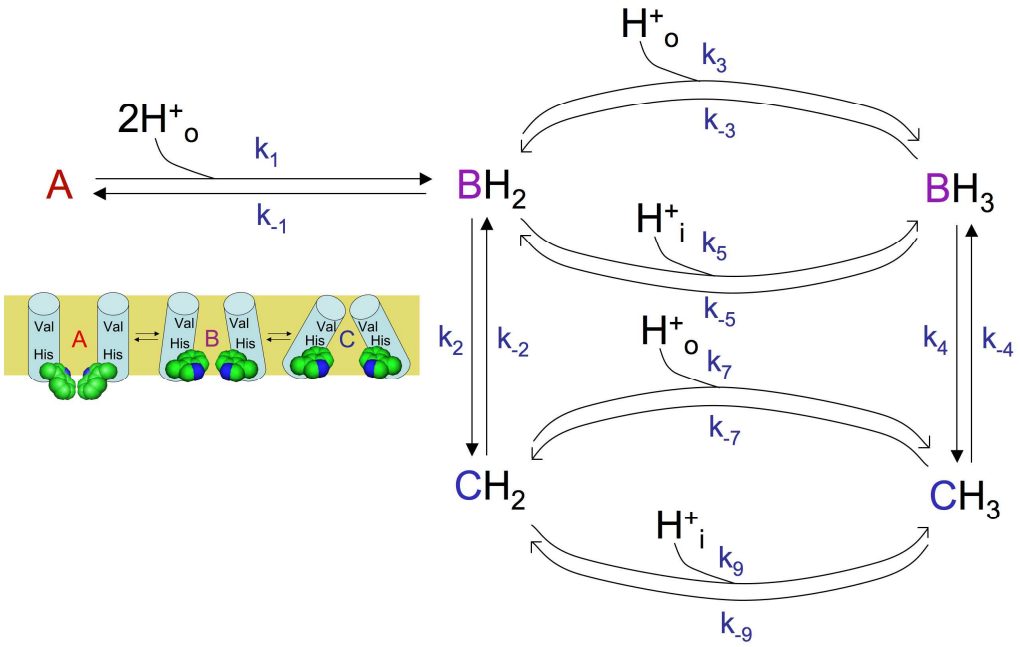

Figure S1. Kinetic scheme used to derive flux equation representing mechanism in Fig. 3; a similar approach was used for the mechanism shown in Fig. 5. A system of equations was constructed where the difference of all rates of formation and depletion of each protein state was set to zero, allowing for the determination of normalized steady-state populations as a function of rate constants (k_i) as well as pH_{in} and $pH_{out,}$. Flux was computed as the difference in proton release and proton binding rates on either side of the membrane under steady-state conditions (see above in Supporting Information). Pairs of rate constants representing non-rate-determining processes could be combined into equilibrium constants, as in Fig. 3 and Fig. 5, although the fitting algorithm employed rate constants only. One rate constant from each kinetic cycle could be eliminated by microscopic reversibility. Certain rate constants were modeled as voltage-dependent (see above in Supporting Information).

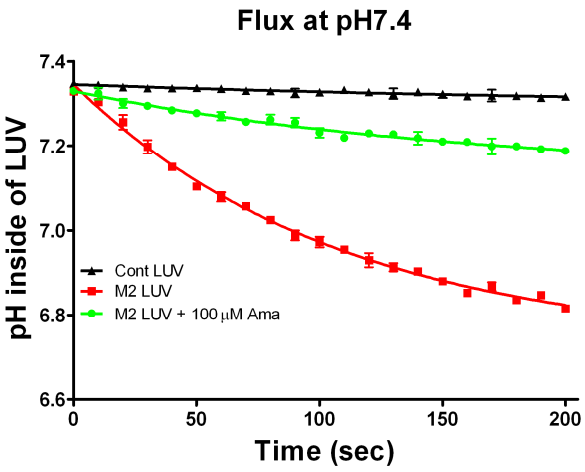

Figure S2. Proteoliposome flux assay demonstrating proton transport activity of the M2 construct used in Trp fluorescence studies when reconstituted under similar conditions. Upon triggering of flux with valinomycin, M2-containing large unilamellar vesicles (M2 LUV, red squares) acidify in an amantadine-sensitive fashion (green circles). Protein-free control vesicles (black triangles) do not show a significant change in pH on the timescale of the experiment.

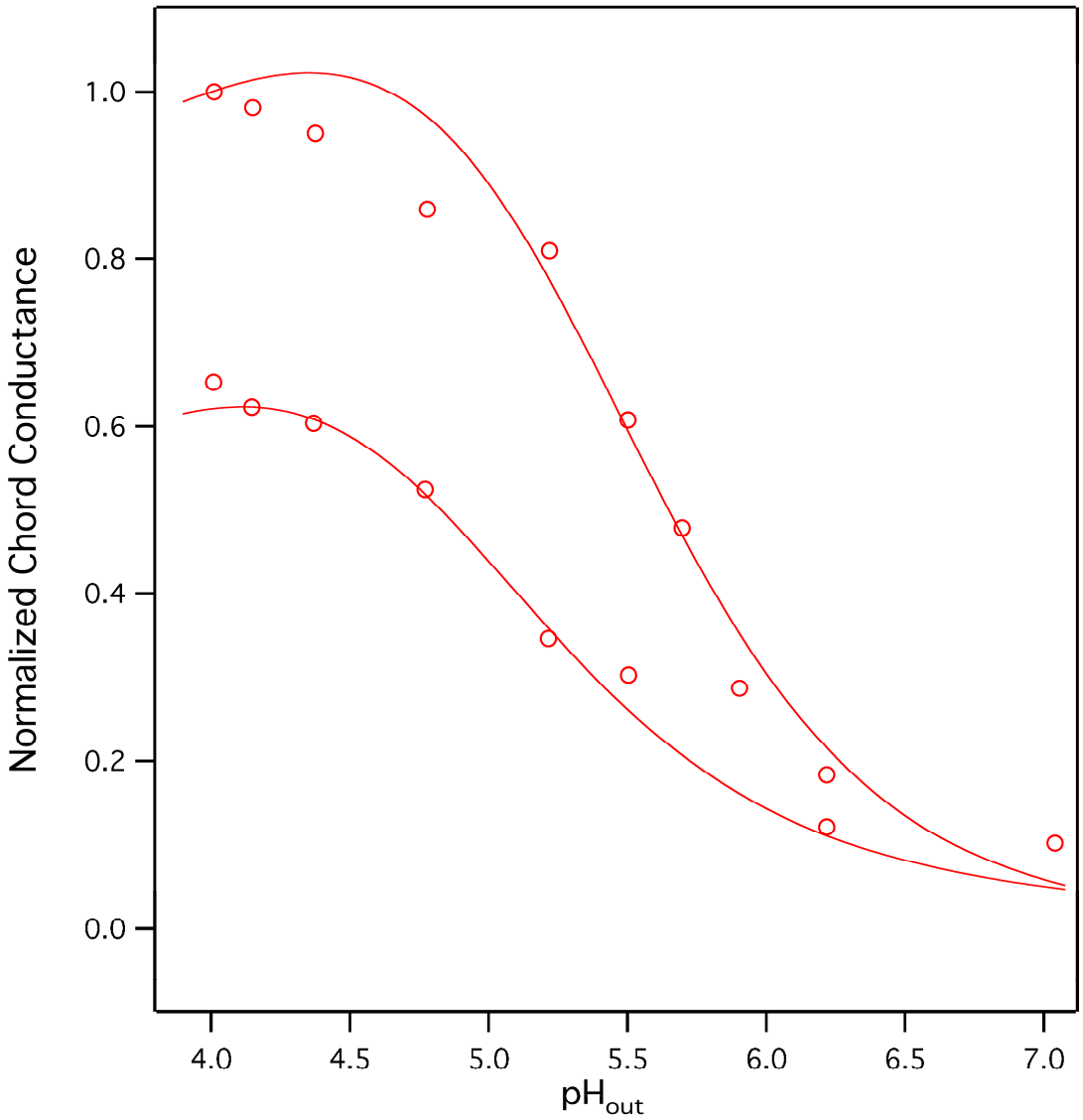

Figure S3. Fit of model in Fig. 3 to M2 chord conductance-pH relationship at -60 mV (upper line and set of points) and +60 mV (lower line and set of points); data from (*4*) and are normalized to pH 4, -60 mV. Chord conductance is defined as current divided by the difference of driving potential and reversal potential (*4*). Data points are based on rimantadine-sensitive net currents. A good fit is obtained to both data sets.

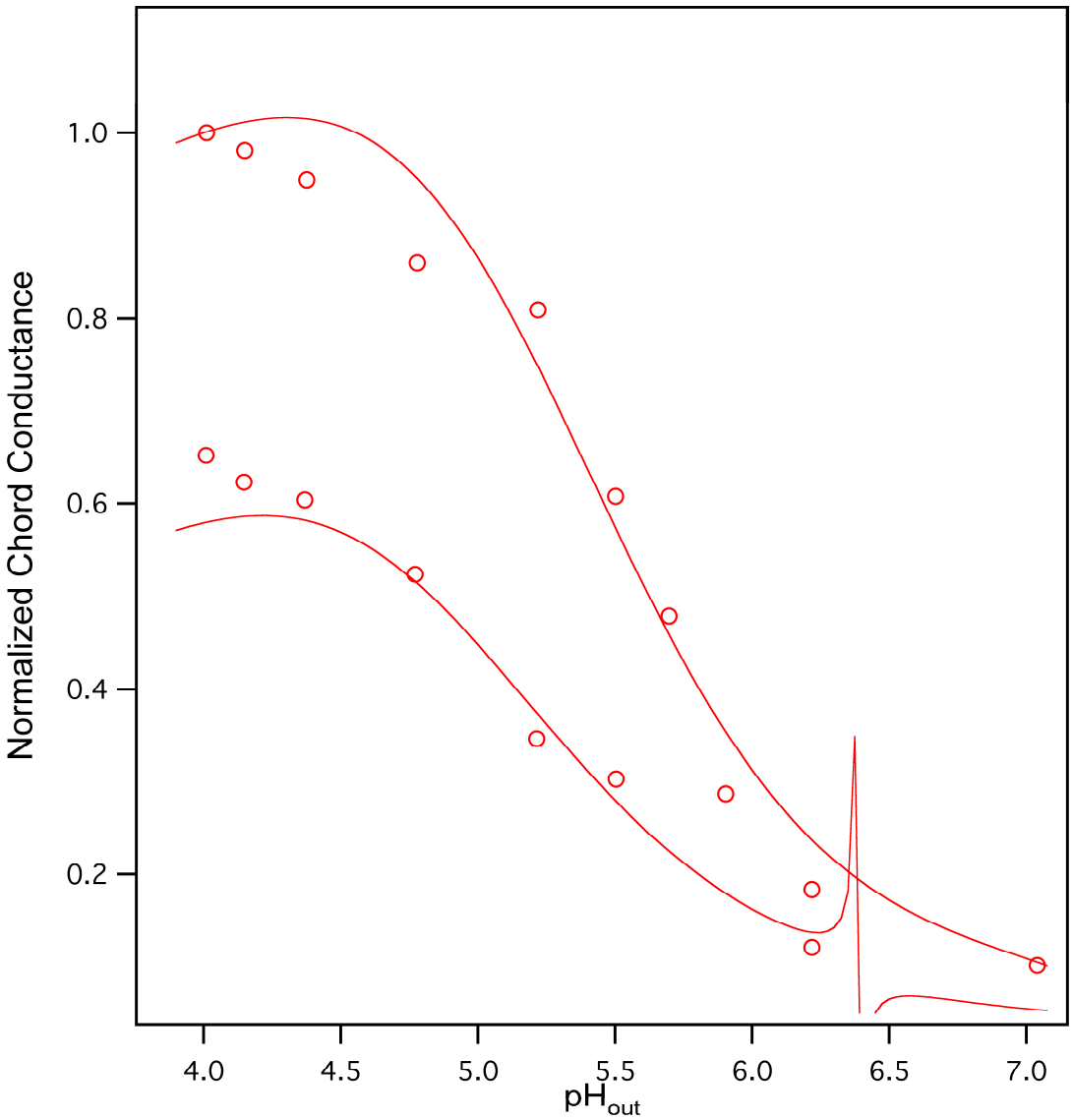

Figure S4. Fit of mechanism shown in Fig. 5 to M2 chord conductance-pH data displayed as in Fig. S3. The predicted function at +60 mV is discontinuous because of software rounding error.

Table S1. Best-fit parameters for mechanism shown in Fig. 3 and Fig. S1. Second column from left, parameters from model guidance with hypothesis that third proton binding favors "C" state ($pK_{aC} > pK_{aB}$). Third column from left, parameters from model guidance with reverse hypothesis. For processes represented as equilibria in Fig. 3 and here, separate rate constants (e.g. as in Fig. S1) were used in the fitting.

Parameter	$pK_{aC} > pK_{aB}$	$pK_{aB} > pK_{aC}$
k_1	5.00E+17	5.00E+17 M^{-2} sec^{-1}
pK_{a1}	1.64E+01	1.64E+01
K2 (toward BH3)	3.39E-01	1.73E+01
k_3	5.60E+06	3.86E+07 M^{-1} sec^{-1}
pK_{a3}	5.99E+00	8.13E+00
K4 (toward CH_3)	1.02E+01	5.73E-02
k_5	0.00E+00	0.00E+00 M^{-1} sec^{-1}
k_7	0.00E+00	0.00E+00 M^{-1} sec^{-1}
k_9	7.41E+08	9.38E+07 M^{-1} sec^{-1}
pK_{a9}	7.47E+00	5.65E+00
Electrical distances (normalized to 1)		
Barrier BH_2 outside prot	2.51E-01	2.52E-01
BH_3 state	2.50E-01	2.55E-01
Barrier BH_3-CH_3	2.50E-01	2.55E-01
CH_3 state	2.52E-01	2.50E-01
Barrier CH_3 inside deprot	4.62E-01	4.67E-01

Table S2. Best-fit parameters for mechanism shown in Fig. 5, presented similarly to Table S1. For sets of rate constants shown as equilibria in Fig. 5, rate constants with positive subscripts correspond to rates in the downward direction in the mechanism figure.

k_1	1.45E+07	sec^{-1}
k_2	9.93E+14	M^{-2} sec^{-1}
pK_{a2}	1.43E+01	
k_3	6.81E+05	sec^{-1}
k_{-3}	5.39E+04	sec^{-1}
k_4	0.00E+00	M^{-2} sec^{-1}
k_5	1.07E+06	sec^{-1}
k_6	9.90E+14	M^{-2} sec^{-1}
pK_{a6}	1.56E+01	
k_7	9.92E+03	sec^{-1}
k_{-7}	1.01E+03	sec^{-1}
k_8	4.07E+06	M^{-1} sec^{-1}
pK_{a8}	5.99E+00	
k_{10}	0.00E+00	M^{-1} sec^{-1}
k_{12}	5.43E+08	M^{-1} sec^{-1}
pK_{a12}	7.49E+00	
Relative electrical distances - first two protons		
Barrier A prot	0.00E+00	
AH_2 state	3.35E-01	
Barrier AH_2-BH_2	3.30E-01	
BH_2 state	4.16E-01	
Barrier BH_2 deprot	9.67E-01	
Relative electrical distances - third proton		
Barrier BH_2 prot	2.04E-01	
BH_3 state	2.08E-01	
Barrier BH_3-CH_3	2.34E-01	

CH_3 state	2.34E-01
Barrier CH_3 deprot	4.62E-01

References:

1. Maxima.sourceforge.net. (2009) Maxima, a Computer Algebra System, 5.18.1 ed.
2. Wolfram Research, I. (2008) Mathematica, 7.0 ed., Wolfram Research, Inc., Champaign, IL.
3. Lear, J. (2003) Proton conduction through the M2 protein of the influenza A virus; a quantitative, mechanistic analysis of experimental data, *FEBS Lett 552*, 17-22.
4. Chizhmakov, I., Geraghty, F., Ogden, D., Hayhurst, A., Antoniou, M., and Hay, A. (1996) Selective proton permeability and pH regulation of the influenza virus M2 channel expressed in mouse erythroleukaemia cells, *J Physiol 494*, 329-336.